Naval Research Laboratory
Washington, DC 20375-5320

NRL/6360/MR—2022/5

Improving the Catalytic Performance of K-Mo2C@Al2O3 for the Reverse Water Gas Shift Reaction

JAMES R. MORSE

HEATHER D. WILLAUER

Scientific Staff
Materials Science & Technology Division

CAMERON F. HOLDER

Materials and Sensors Branch
Materials Science & Technology Division

JEFFREY W. BALDWIN

Functional Materials and Energy Section
Acoustics Division

October 11, 2022

REPORT DOCUMENTATION PAGE

Form Approved
OMB No. 0704-0188

1. REPORT DATE *(DD-MM-YYYY)*	**2. REPORT TYPE**	**3. DATES COVERED** *(From - To)*
11-10-2022	NRL Memorandum Report	10/01/2021 – 09/27/2022

4. TITLE AND SUBTITLE

Improving the Catalytic Performance of K-Mo2C@Al2O3 for the Reverse Water Gas Shift Reaction

5a. CONTRACT NUMBER

5b. GRANT NUMBER

5c. PROGRAM ELEMENT NUMBER

6. AUTHOR(S)

James R. Morse, Cameron F. Holder, Jeffrey W. Baldwin, and Heather D. Willauer

5d. PROJECT NUMBER

5e. TASK NUMBER

5f. WORK UNIT NUMBER
1P96

7. PERFORMING ORGANIZATION NAME(S) AND ADDRESS(ES)

Naval Research Laboratory
4555 Overlook Avenue, SW
Washington, DC 20375-5320

8. PERFORMING ORGANIZATION REPORT NUMBER

NRL/6360/MR--2022/5

9. SPONSORING / MONITORING AGENCY NAME(S) AND ADDRESS(ES)

Naval Research Laboratory
4555 Overlook Avenue, SW
Washington, DC 20375-5320

10. SPONSOR / MONITOR'S ACRONYM(S)

NRL 6.1 Base Program

11. SPONSOR / MONITOR'S REPORT NUMBER(S)

12. DISTRIBUTION / AVAILABILITY STATEMENT

DISTRIBUTION STATEMENT A: Approved for public release; distribution is unlimited.

13. SUPPLEMENTARY NOTES

14. ABSTRACT

The reduction of CO2 to CO through the reverse water gas shift (RWGS) reaction is an important catalytic step in the in the overall strategy of CO¬2 utilization. The product CO can be subsequently used as a feedstock for a variety of useful reactions, including the synthesis of fuels through the Fischer-Tropsch process. Recent works have demonstrated that potassium promoted molybdenum carbide (K-Mo2C) is a highly selective catalyst for low-temperature RWGS. In this work, we describe the systematic investigation of key parameters in the synthesis of K-Mo2C, and their influence on the overall activity and selectivity for the low-temperature RWGS reaction. Specifically, we demonstrate how catalyst support, precursor calcination, carburization conditions, catalyst loading, and long-term ambient storage influence performance of the K-Mo2C catalyst.

15. SUBJECT TERMS

CO2 hydrogenation
Heterogeneous catalysts
Molybdenum carbide
Reverse water gas shift

16. SECURITY CLASSIFICATION OF:			**17. LIMITATION OF ABSTRACT**	**18. NUMBER OF PAGES**	**19a. NAME OF RESPONSIBLE PERSON**
a. REPORT	**b. ABSTRACT**	**c. THIS PAGE**			James R. Morse
U	U	U	U	20	**19b. TELEPHONE NUMBER** *(include area code)* (202) 404-3418

Standard Form 298 (Rev. 8-98)
Prescribed by ANSI Std. Z39.18

This page intentionally left blank.

Contents

This page intentionally left blank.

EXECUTIVE SUMMARY

The reduction of CO_2 to CO through the reverse water gas shift (RWGS) reaction is an important catalytic step in the in the overall strategy of CO_2 utilization. The product CO can be subsequently used as a feedstock for a variety of useful reactions, including the synthesis of fuels through the Fischer-Tropsch process. Recent works have demonstrated that potassium promoted molybdenum carbide (K-Mo_2C) is a highly selective catalyst for low-temperature RWGS. In this work, we describe the systematic investigation of key parameters in the synthesis of K-Mo_2C, and their influence on the overall activity and selectivity for the low-temperature RWGS reaction. Specifically, we demonstrate how catalyst support, precursor calcination, carburization conditions, catalyst loading, and long-term ambient storage influence performance of the K-Mo_2C catalyst.

1.0 Background

Sustainable conversion of CO_2 into fungible liquid fuels represents an attractive alternative (or potential complement) to fossil-based fuel production. In addition to the obvious environmental merits, such a process would enable the production of fuels independent of the logistical burden of fossil fuel refinement and delivery. The orchestration of sustained liquid fuel delivery is of key importance to the U.S. DOD and its allies, as it directly impacts "Freedom of Action" for the Warfighter.[1,2] Accordingly, CO_2 to fuel technologies have been identified as an important focus area, which would enable strategic advantages.[3]

To address this, the U.S. Naval Research Laboratory is currently developing a process capable of producing hydrocarbon fuels using CO_2 and H_2 extracted from seawater.[4–10] A critical step in this process is the thermocatalytic reduction of CO_2 to more reactive intermediates that can be subsequently hydrogenated to useable chemicals and fuels. The reduction of CO_2 to CO through the endothermic reverse water gas shift reaction (RWGS)(eq. 1) is a promising pathway, as the intermediate CO can be further hydrogenated to usable fuels through the well-developed Fischer-Tropsch process.[11–14]

$$(1)\quad CO_2 + H_2 \leftrightarrow CO + H_2O, \Delta H^0{}_{298\,K} = 41.2\ kJ\ mol^{-1}$$

High CO_2 conversions and CO selectivities can be readily achieved when the RWGS reaction is operated at high temperatures (>800 °C), however, these temperatures can lead to catalyst degradation, safety concerns, and pose limitations to the design and operation of reactors.[15–17] For these reasons, RWGS catalysts capable of operating at lower temperatures (250-350 °C) are desirable. Unfortunately, at these temperatures the RWGS reaction is equilibrium limited (16-35% conversions at a 3:1 ratio of H_2:CO_2) and competes with the thermodynamically favored methanation of CO_2 and CO, further decreasing CO yields.[11,12] While the equilibrium limitations of low-temperature RWGS can be overcome by removing the product water, and recycling the remaining reactor effluent over the RWGS catalyst,[18,19] low temperature RWGS catalysts must demonstrate high CO selectivity to efficiently utilize CO_2 and H_2 feedstocks.

Transition metal carbides (TMCs) have been identified as affordable and effective catalysts for a variety of chemical transformations including CO oxidation, methane reforming, hydrogenation and RWGS.[20–23]

Manuscript approved September 19, 2022.

The addition of chemical promoters to TMCs can further improve catalytic performance by attenuating the material's chemical and structural properties, enabling improved activities and/ or selectivites.[24,25] Recent works by our lab and others have demonstrated that the addition of potassium promoters drastically improve the low temperature RWGS selectivity of TMCs without sacrificing the overall activity of the catalyst.[26,27] Specifically, potassium promoted molybdenum carbide supported on high surface area gamma alumina (K-Mo_2C@γ-Al_2O_3) has demonstrated excellent performance over a range of temperatures, operating conditions, and reactor scales.[19,27,28] Optimization of the K-Mo_2C catalyst synthesis is critical to determine how synthetic details can influence important properties, such as catalyst distribution, active surface area, promotional effects, attrition rate, and catalyst-support interactions.[29,30] While previous works have addressed the relationship between potassium content and catalyst performance,[27] further systematic investigations focusing K-Mo_2C preparation as it pertains to catalyst activity have yet to be reported. In this work, we investigate the influence of key variables on the performance of the K-Mo_2C RWGS catalyst including catalyst loading, calcination temperature, carburization conditions, the influence of pH on the catalyst synthesis, the influence of the γ-Al_2O_3 support, as well as the effects of long-term catalyst storage under ambient conditions (shelf life).

2.0 Objective

The objective of this work is to improve the catalytic performance of potassium promoted molybdenum carbide (K-Mo_2C) for the reverse water gas shift reaction, so that CO_2 can be more efficiently used as a feedstock for the synthesis of Navy relevant chemicals and fuels. To accomplish this objective, we systematically study the influence of various synthetic protocols as it pertains to catalyst stability and performance. The results of these experiments are rationalized and discussed to provide a better understanding of catalyst design for the reverse water gas shift reaction.

3.0 Experimental:

3.1 Materials

Ammonium molybdate tetrahydrate ($(NH_4)_6Mo_7O_{24} \cdot 4H_2O$) 81.0-83.0% MoO_3 basis, and potassium carbonate (K_2CO_3) >99% were purchased from Sigma Aldrich. γ-Al_2O_3 powder (> 97%) was purchased from STREM Chemicals. All gases used for catalyst synthesis and testing were supplied from Matheson.

3.2 Catalyst Preparation

3.2.1. Typical catalyst preparation

The Mo based catalysts were synthesized by the evaporation deposition method. In a typical synthesis, γ-Al_2O_3 powder was added to a beaker of deionized water, followed by ammonium molybdate tetrahydrate, and potassium carbonate (when applicable). The solution was then stirred at 60 °C for 48 hours to allow for complete evaporation of water. Unless otherwise noted, the materials were then calcined in air using a muffle furnace at 350 °C for 12 hours. Finally, following calcination, the materials were carburized in 4-gram batches, using a tube furnace flowing a blend of 20% methane and 80% hydrogen gas at 300 mL min^{-}

[1] for a total of 4 hours at 600 °C. Following carburization, the samples were passivated at ambient temperature under flowing a blend of 1% oxygen and 99% nitrogen at 10 mL min^{-1} overnight.

3.2.2. Unsupported catalyst preparation

For the preparation of unsupported Mo and K-Mo catalysts, the procedure described in section 2.2.1. was followed, except γ-Al_2O_3 was not added during the evaporation deposition method.

3.3 X-Ray Diffraction (XRD)

Measurements were performed on a Rigaku Smartlab X-ray diffractometer using Cu Kα monochromated radiation operated at 40 kV and 44 mA at room temperature over the range of 10-80° 2θ. X-ray diffraction patterns for the catalysts were referenced to reported patterns from multiple databases. Average crystallite size was estimated by performing Scherrer analysis using the (101) reflection of Mo_2C at 39.5° 2θ.

3.4 BET Surface Area Analysis

Nitrogen adsorption analysis was performed at −196 °C, using a Beckman-Coulter S.A. 3100 Surface Area Analyzer. Prior to the measurement, the catalyst was degassed at 120 °C for 30 min under 4 μmHg vacuum. To account for any temperature induced changes to the catalyst support, the bare γ-Al_2O_3 was calcined, pelletized and heated under the same carburizing atmosphere as the Mo_2C catalysts before BET characterization.

3.5 Thermogravmetric Analysis (TGA)

The TGA experimental setup consisted of a Q500 TGA (TA Instruments). In a typical run, approximately 15 mg of sample was added to an alumina boat, which was then purged with N_2 gas for 90 min at a flow rate of 200 mL min^{-1} at room temperature. Following the N_2 purge, the sample was heated to 975 °C at a rate of 5 °C min^{-1}, under a flowing air atmosphere.

3.6 Reactor Studies

Prior to testing, the catalysts were pelletized under a force of 1 ton for 10 min, then ground and sieved to a particle size of 200–350 μm to improve mass transfer. For a typical experiment, 0.5 g of catalyst pellets were loaded into a 0.25 in stainless-steel reactor. The catalyst bed was reduced under H_2 at 300 °C and 0.5 MPa at a flow rate of 50 mL min^{-1} for a total of 2.5 h. The catalyst bed was then isolated as the rest of the reactor system was pressurized to 2.0 MPa with a blend of N_2, CO_2, and H_2 gases at ratios commensurate with the experimental flow rates. Once pressurized, the reactant gases were introduced to the catalyst bed at a 3:1 H_2:CO_2 ratio, with flowrates corresponding to the reported gas hourly space velocities (GHSV). N_2 was used as an internal standard to quantify CO_2 conversion and CO yield, and represented 16% of the reagent gas blend. Reactant flowrates were controlled using programmable mass flow controllers (Brooks SLA5850). Reactions were monitored by gas chromatography (Agilent 7890A), and all reported data were recorded after steady state had been achieved. Carbon balances between 95-100% were observed for all reported reactor data.

4.0 Results and Discussion:

4.1 Influence of γ-Al_2O_3 Support

To develop a baseline for Mo_2C performance, and to evaluate the influence of the high surface area γ-Al_2O_3 support on the catalytic activity of K-Mo_2C, the potassium promoted molybdenum (K-Mo) precursor was carburized, with and without the γ-Al_2O_3 support. For comparison, the same procedures were also carried out on identical precursors in absence of the potassium promoter. The four catalysts were prepared under identical conditions, and consisted of molar ratios of 1/4/15 (K/Mo/γ-Al_2O_3). Figure 1 displays the X-ray diffraction patterns for the resulting materials. The K-Mo precursor supported on the γ-Al_2O_3 was fully carburized to yield the Mo_2C phase. Likewise, when the potassium promoter was excluded, the same Mo_2C phase was observed with and without the γ-Al_2O_3 support, although the signal corresponding to this phase was significantly less prominent for the γ-Al_2O_3 supported catalyst. Notably, however, when the unsupported K-Mo precursor is treated under identical conditions in the absence of the γ-Al_2O_3 support, the unsupported material was reduced to metallic molybdenum.

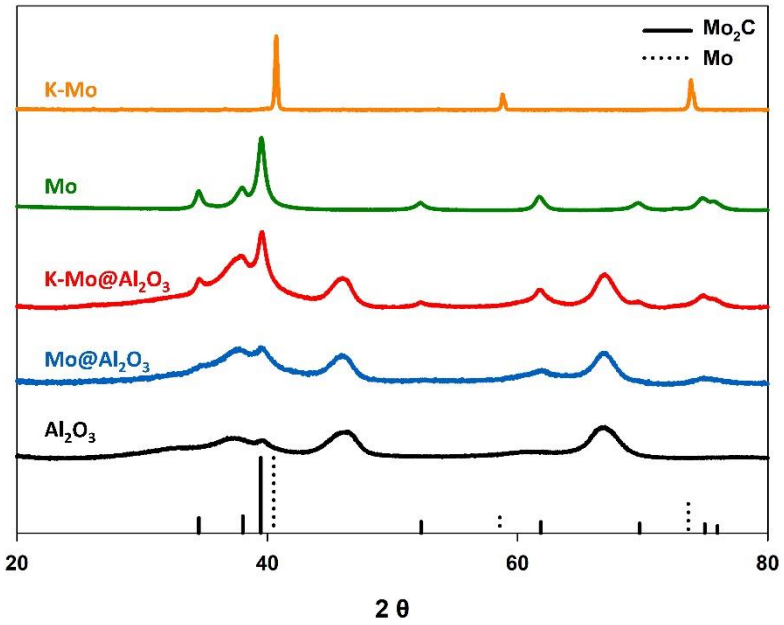

Figure 1. X-ray diffraction patterns for the various molybdenum-based catalysts, with and/or without the potassium promoter and γ-Al_2O_3 support. Reference patterns for both Mo_2C (solid line) and metallic Mo (dotted line).

Reduction of the unsupported K-Mo precursor to metallic Mo is likely due to the presence of the alkali dopant, which has been reported to inhibit the carburization of molybdenum species.[31,32] It is therefore interesting to note that, under identical conditions, the presence of the γ-Al_2O_3 support appears to inhibit complete reduction of the impregnated K and Mo precursors, enabling straightforward carburization to the Mo_2C phase. This may be due to the high surface area of Al_2O_3, which allows for dispersion of the K and Mo precursors across the support, thereby limiting the physical interaction between the impregnated

precursors. Alternatively, the direct carburization of the K-Mo-Al_2O_3 precursor may be due to interaction between the support and impregnated species, which is known to influence the temperatures of various chemical transformations.[33–36]

The specific surface areas of the various catalysts were calculated using N_2 physisorption, and are displayed in Table 1, along with the measured activity, selectivity and overall CO yield for the reverse water gas shift reaction at 300 °C. Under the conditions tested, the RWGS reaction is thermodynamically limited to CO yields of 23%.

Table 1: Performance of Mo-based catalysts with and without γ-Al_2O_3 and potassium promoter. All catalysts were tested under the following conditions: 3:1- H2:CO_2 ratio at 300 °C and at a GHSV of 1 mL g^{-1} s^{-1}.

Starting Material	Mo Phase Following Carburization	BET Surface Area (m^2g^{-1})	CO_2 Conv. (%)	CO Selectivity (%)	CO Yield (%)
			300 °C, 3:1 H_2:CO_2, GHSV: 1 mL $g^{-1}s^{-1}$		
K-Mo *(1/4)*	Metallic Mo	1.0	0.0	N.A.	N.A.
K-Mo@γ-Al_2O_3 *(1/4/15)*	Mo_2C	142.4	20.0	93.0	18.6
Mo	Mo_2C	13.7	32.6	8.2	2.7
Mo@γ-Al_2O_3 *(4/15)*	Mo_2C	154.1	18.7	73.1	13.7
Bare γ-Al_2O_3	N.A.	160.0	N.A.	N.A.	N.A.

As expected, the K-promoted catalysts displayed the highest selectivity for the product CO, and a clear correlation was observed between surface area and RWGS activity, with the K-Mo_2C@γ-Al_2O_3 displaying the highest overall CO yield. The unsupported Mo_2C was measured to have a surface area of 13.7 m^2 g^{-1} and exhibited surprisingly large CO_2 conversions, but poor selectivity for the desired RWGS reaction. The unsupported K-promoted catalyst exhibited the lowest surface area of 1.0 m^2 g^{-1}, and exhibited no observable CO_2 conversion under the conditions tested. The lack of activity for the unsupported K-promoted catalyst demonstrates that, under the synthetic conditions explored in this work, efficient K-promoted molybdenum catalysts cannot be accessed without the γ-Al_2O_3 support.

4.2 Calcination

To understand the influence of calcination on the catalyst precursors, thermogravimetric analysis (TGA) was employed. Figure 2 shows the mass loss and the corresponding differential of mass loss for various combinations of the Mo and K precursors with and without the Al_2O_3 support when heated under air. For the unsupported Mo precursor, mass loss ceases above 350 °C, indicating complete oxidation to the MoO_3 phase. In contrast, the unsupported K-Mo precursor exhibits a different mass loss curve, with complete oxidation occurring at about 400 °C. The mass loss curves for the two precursor combinations supported on Al_2O_3 are more difficult to interpret, as the Al_2O_3 makes up the majority of the sample mass, but differences in the thermal oxidation of these samples can still be discerned from the differentials of their respective TGA curves shown in the inset of Figure 2b. Together, the four curves in Figure 2a and 2b demonstrate distinctly different patterns of thermally induced oxidation, indicating that the K-precursor, Mo-precursor, and Al_2O_3 support interact during calcination to generate different species. This is supported by X-ray diffraction patterns for the various precursors following calcination, which are shown in Figure 3. A variety of different molybdenum containing crystalline phases, including MoO_3, $K_2Mo_4O_{13}$,

$Al_2(MoO_4)_3$, and $KAl(MoO_4)_3$, were observed for the various combinations of K precursor, Mo precursor and Al_2O_3 support, demonstrating that these precursor materials will interact upon thermal treatment.

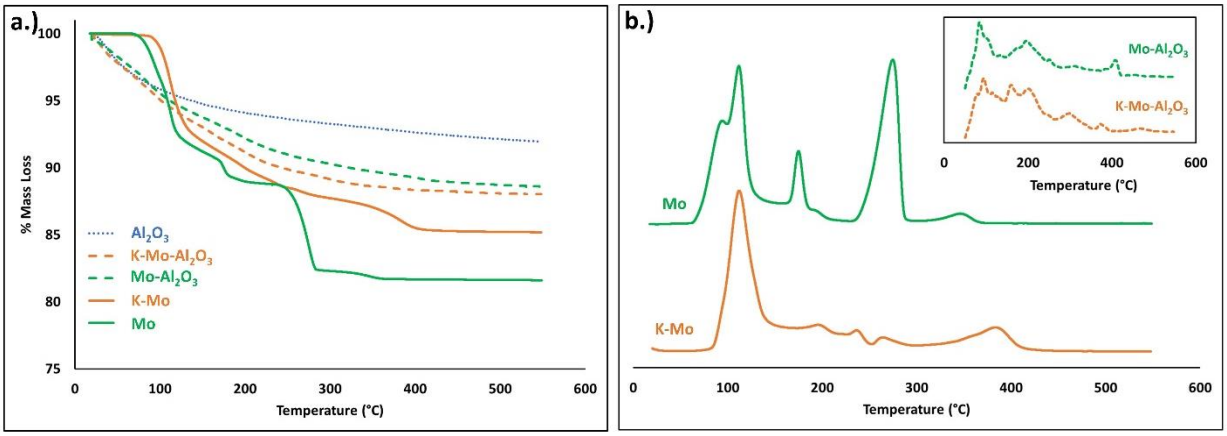

Figure 2: a) Mass loss curves for catalyst precursors Mo, K-Mo, Mo-Al_2O_3, and K-Mo-Al_2O_3 when heated under air. b) Differential of mass loss curves shown Figure 2a. The inset of Figure 2b shows the differential mass loss curves for the two Al_2O_3 supported samples.

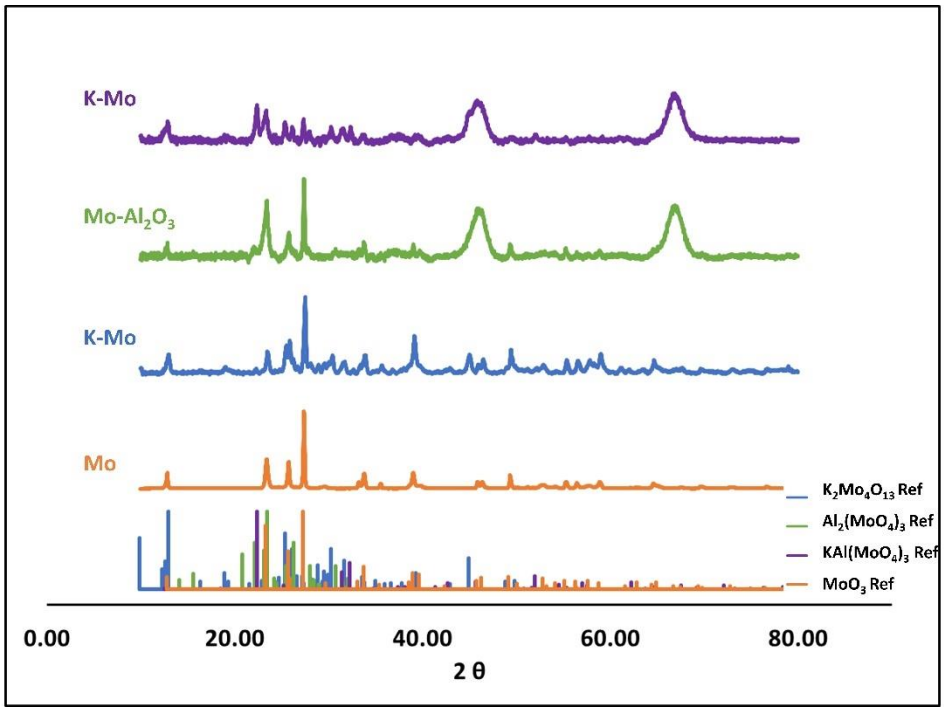

Figure 3: X-ray diffraction patterns for the various combinations of precursors K, Mo and Al_2O_3 following calcination. Reference patterns for the corresponding oxides are color coded to the patterns they match best. Note: the two broad peaks at 45 and 68 2θ correspond to the Al_2O_3 support.

The temperature programmed carburization of transition metal oxides using gaseous reactants is a convenient and well-known route to yield high surface area carbides.[22,37–39] Accordingly, in previous

works, K-Mo_2C@γ-Al_2O_3 was prepared though a three-step process: 1.) Impregnation of metal salts onto the γ-Al_2O_3 support, 2.) Calcination of the precursors to the respective metal oxides, and 3.) Temperature programed carburization of the supported oxides. To understand the influence of calcination on catalyst performance, K-Mo_2C@γ-Al_2O_3 samples were prepared using three different calcination methods prior to carburization: a.) no calcination, b.) calcination at 350 °C, and c.) calcination at 425° C. All other synthetic procedures were identical.

Figure 4 shows overlaid X-ray diffraction patterns (normalized to the γ-Al_2O_3 support) for the resulting K-Mo_2C@γ-Al_2O_3 samples, and Table 2 shows the corresponding RWGS activity and selectivity at two different gas hourly space velocities (GHSV). Following carburization, the Mo_2C phase was observed for all three samples. A slight decrease in the intensity of the XRD signal corresponding to the Mo_2C phase was observed as a function calcination temperature, with the "no calcination" sample exhibiting the most prominent Mo_2C pattern. The CO yield for the RWGS reaction also decreased as a function of increasing calcination temperature, with the "no calcination" sample exhibiting the greatest activity and CO yield. The differences in catalyst performance were more pronounced at greater reagent flowrates (GHSV: 5mL g^{-1} s^{-1}). Although not observable by XRD, calcination likely drives the formation of oxidized species that cannot be readily carburized under the conditions tested in this work, thereby reducing the overall quantity of Mo_2C active sites available to catalyze the RWGS reaction. Together, these data demonstrate that calcination of the K-Mo precursor prior to carburization is unnecessary, and in fact detrimental, to the performance of the K-Mo_2C RWGS catalysts.

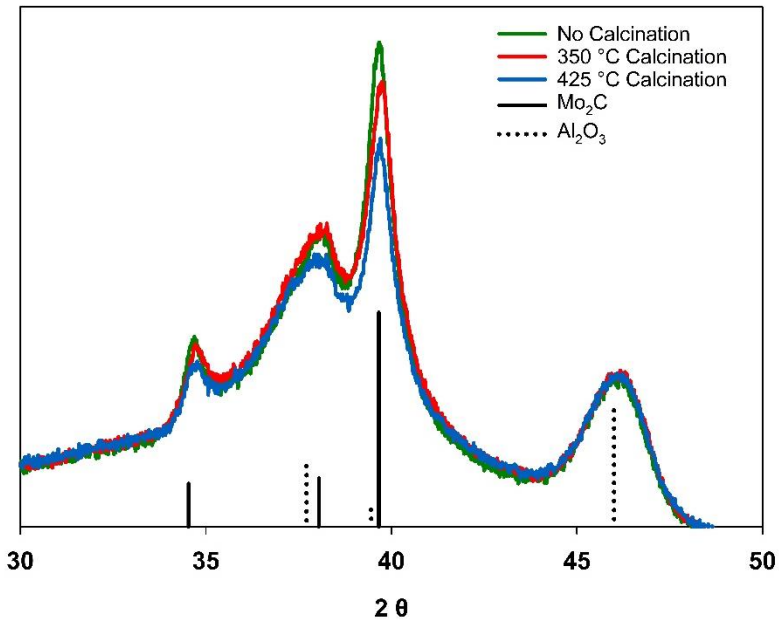

Figure 4. Normalized X-ray diffraction patterns for K-Mo_2C@γ-Al_2O_3 prepared at different calcination temperatures.

Table 2. RWGS activity for K-Mo_2C@γ-Al_2O_3 prepared using different calcination temperatures. All catalysts were tested under the following conditions: 3:1- H_2:CO_2 ratio at 300 °C.

K-Mo_2C@γ-Al_2O_3	CO_2 Conv. (%)	CO Selectivity (%)	CO Yield (%)	CO_2 Conv. (%)	CO Selectivity (%)	CO Yield (%)
	GHSV: 1 mL g^{-1} s^{-1}			GHSV: 5 mL $g^{-1}s^{-1}$		
No calcination	20.6	90.6	18.7	14.1	97.2	13.7
350 °C calcination	20.0	93.0	18.6	12.5	98.0	12.3
425 °C calcination	18.5	94.0	17.4	10.0	97.6	9.8

4.3 Effect of Carburization Time

While the temperature programmed carburization of metal oxide precursors is a convenient way to generate high surface area transition metal carbides, the time scale and temperature of carburization can have important ramifications in the final material properties. For example, under certain conditions, the presence of methane gas in the carburizing stream can lead to the deposition of polymeric carbon across the surface of the carbide, significantly reducing the catalytically active surface area.[26,38,40] Accordingly, care should be taken to ensure complete carburization of the metal oxide precursors, while minimizing or eliminating polymeric surface carbon. Previous procedures have followed carburization with a subsequent "hydrogen treatment" step, in which the freshly carburized sample is exposed to 100% flowing H_2 at 600 °C for one hour. This hydrogen treatment is intended to remove any polymeric carbon from the catalyst surface.[27]

To probe the influence of carburization time on the generation of K-Mo_2C@γ-Al_2O_3 catalysts, identical K-Mo@γ-Al_2O_3 precursors were carburized under various time scales and gas flow rates. Table 3 lists the resulting phases obtained for K-Mo@Al_2O_3 precursors carburized under 20% CH_4 in H_2 at 600 °C at varying gas flows and with or without a subsequent treatment in 100% H_2 at 600 °C. For reference, the respective RWGS activity and selectivities for these catalysts are also included in Table 3, and the resulting X-ray diffraction patterns for the materials are shown in Figure 5.

As can be seen in Figure 5, when the precursor is carburized at the lowest total gas flow of 0.75 L g^{-1} (with a subsequent H_2 step), MoO_2 is the primary phase observed, indicating incomplete reduction/carburization. When the precursor was carburized using a total gas flow of 3 L g^{-1}, followed by a subsequent H_2 treatment step, the resulting material exhibited diffraction peaks corresponding to both MoO_2 and metallic Mo phases, again indicating incomplete carburization. When the precursor is carburized using an extremely high total gas flow of 140 L g^{-1}, and not subsequently introduced to a hydrogen treatment step, the resulting material displays diffraction peaks corresponding exclusively to Mo_2C. The catalytic activity for this fully carburized sample was observed to be the greatest of the samples listed in Table 3, indicating that extensive carburization times at 600 °C do not lead to polymeric carbon deposition or reduced catalyst activity. This is in line with previous thermodynamic calculations, which predict polymeric carbon deposition will occur at and above 640 °C at 20% CH_4 in H_2.[40]

Subsequent experiments, the details of which are beyond the scope of this report, have led to the development of a standard operating procedure for the complete carburization of K-Mo@Al_2O_3

precursors. This consists of carburizing 4 g of precursor in 20% CH_4 in H_2 at 600 °C, at a total gas flow rate of 0.3 L min^{-1} for a total of 4 hours (corresponding to a total gas flow of 18 L g^{-1}). It has also been determined that, under these conditions, subsequent hydrogen treatment steps do not improve catalyst performance.

Table 3. Molybdenum phases as detected by X-Ray diffraction for the K-Mo@Al_2O_3 precursor after carburization at varying gas flows, and with or without a subsequent "H_2 treatment" step. Carburization conditions: 600 °C, 20% CH_4 in H_2. CO_2 conversions and CO selectivites are also shown for the RWGS at 3:1 H_2:CO_2, 2.0 MPa, and 300 °C.

Gas Flow	H_2 Treatment	Phase	CO_2 Conv (%)	CO Selectivity (%)
			GHSV: 2.7 mL $g^{-1}s^{-1}$	
0.75	Yes	MoO_2	N.A.	N.A.
3	Yes	MoO_2, Mo, Mo_2C	3.5	99.0
140	No	Mo_2C	15.5	96.1

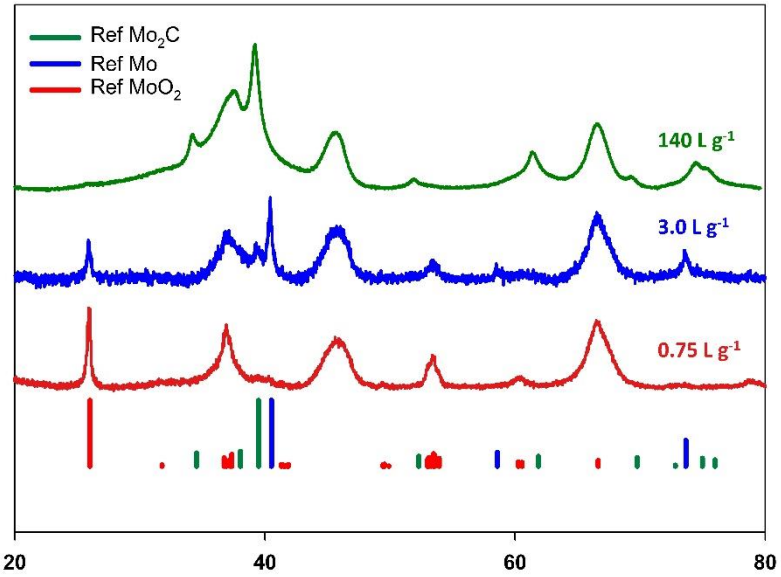

Figure 5. X-Ray diffraction patterns following carburization of the K-Mo@Al_2O_3 precursor under varying gas flows.

4.4 Catalyst Loading

In an attempt to further optimize the overall performance of the K-Mo_2C catalyst for RWGS, the quantity of promoter and catalyst loaded onto the γ-Al_2O_3 support was varied. All catalysts were directly carburized following impregnation (no calcination step). Table 4 shows the overall CO_2 conversion and CO selectivities for the RWGS reaction for four K-Mo_2C@γ-Al_2O_3 catalysts prepared at differing K/Mo/Al_2O_3 molar ratios: *(1/4/30)*, *(1/4/15)*, *(1/4/7.5)*, and *(1/8/15)*.

(1/4/30) displayed a CO_2 conversion of 6.9%, and an overall CO yield of 6.6%, the lowest activity observed of the variously loaded K-Mo_2C@γ-Al_2O_3 catalysts. *(1/4/15)* displayed a CO_2 conversion of 14.1%, and an overall CO yield of 13.7%, demonstrating the greatest activity of the catalysts listed in Table 4. The

catalysts with higher loadings, *(1/4/7.5)* and *(1/8/15)*, displayed CO_2 conversions of 11.5 and 13.1, and overall CO yields of 11.4 and 12.7, respectively.

Figure 6 shows the resulting X-ray diffraction patterns for the K-Mo_2C@γ-Al_2O_3 catalysts of differing loadings. Notably, the Mo_2C phase was not observed for the *(1/4/30)* sample, indicating the Mo species were of low surface density, and were finely dispersed across the γ-Al_2O_3 support. However, reflections corresponding to Mo_2C were observed for the other three samples, with the reflection intensities increasing with Mo loading. The average crystallite size of the Mo_2C species were calculated through Scherrer analysis, and found to be 9 nm, 17 nm, and 16 nm for *(1/4/15)*, *(1/4/7.5)*, and *(1/8/15)*, respectively. These calculations, along with the RWGS activity reported in Table 3, suggest that Mo loadings above a molar ratio of 4/15 (Mo/Al_2O_3), do not produce more active surface sites due to increased Mo_2C particle size.

Table 4. Average crystallite size as calculated by Scherrer analysis, and RWGS activity for K-Mo_2C@γ-Al_2O_3 catalysts of various loadings. All catalysts were tested under the following conditions: 3:1- H_2:CO_2 ratio at 300 °C and at a GHSV of 5 mL g^{-1} s^{-1}.

Catalyst (K/Mo/Al_2O_3) Molar Ratio	Scherrer Crystallite Size (nm)	CO_2 Conv. (%)	CO selectivity (%)	CO yield (%)
		GHSV: 5 mL g^{-1} s^{-1}		
(1/4/30)	N.A.	6.9	95.5	6.6
(1/4/15)	9	14.1	97.2	13.7
(1/4/7.5)	17	11.5	98.8	11.4
(1/8/15)	16	13.1	97.0	12.7

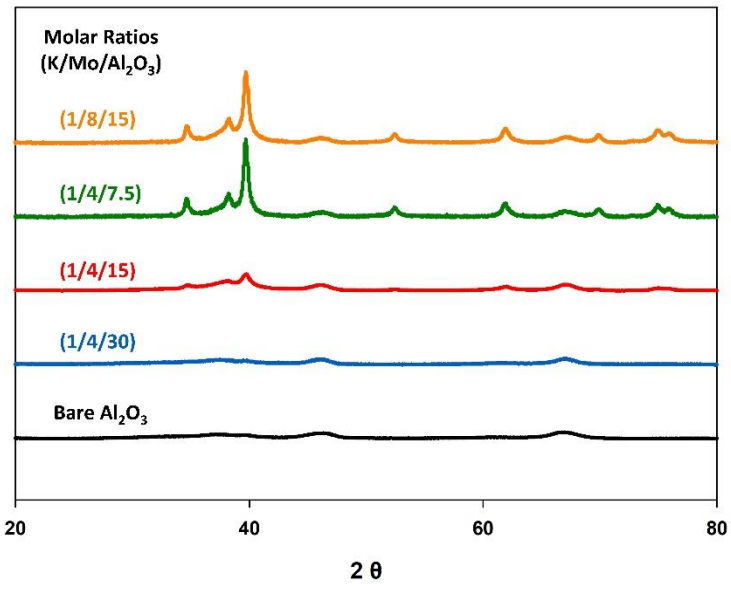

Figure 6. Normalized X-ray diffraction patterns for the K-Mo_2C@γ-Al_2O_3 of various precursor loadings.

4.5 Influence of Impregnating Solution pH on Catalyst Activity:

With respect to catalysts synthesized by "wet impregnation" or "evaporation-deposition" methods, some authors have reported a correlation between the pH of the impregnating solution and the resulting catalyst activity.[30,41–44] These trends are rationalized by charge differences between the surface of the support, and the dissolved metal salts while in solution. It is believed that typically, negatively charged salts will favorably interact with the support when the pH of the solution is below the point of zero charge (PZC) of the support and that positive ions will favorably interact when the pH is above the PZC of the support. In this case, the molybdate species in the impregnating solution are negatively charged, and the point of zero charge for Al_2O_3 is at a pH between 7-8.[30,45] In an attempt to improve activity of the K-Mo_2C for the RWGS reaction, the pH of the impregnating solution was altered by adding dilute nitric acid, and compared to a traditionally synthesized catalyst under identical conditions.

Both catalyst samples were synthesized at a 1/4/15 molar ratio of K/Mo/Al_2O_3 as described in the Experimental Section (Section 2.2.1). A pH probe was used to monitor the pH of the solution after the addition of each reactant. After addition of 10 g of Al_2O_3 support to 200 mL deionized water, the pH was measured to be 7.3. Following addition of 4.6 g ammonium molybdate precursor, the pH dropped to 5.5, and then rose to 5.9 following addition of 0.45 g of potassium carbonate. To increase the interaction between the Al_2O_3 surface and the negatively charged molybdate species, we attempted to further protonate the Al_2O_3 surface with the addition of nitric acid (HNO_3). 191mL of a 0.1 M HNO_3 solution was added dropwise to the impregnating solution to yield a final pH of 4.0. The solution was allowed to evaporate overnight, then was carburized and pelletized as described previously.

Table 5 lists the pH of the impregnating solution for a "standard synthesis", as well as for an "acidified synthesis", along with the measured activity and selectivity of the two catalysts for the RWGS under identical conditions. The measured activities and selectivites under the two different flow rates showed little difference between catalyst samples, indicating that, in this case, the pH of the impregnating solution does not play a major role in the overall catalyst performance.

Table 5. pH of the impregnating solution, along with the corresponding activity and selectivity for the resulting catalysts measured under two different GHSVs. All catalysts were tested under the following conditions: 3:1- H_2:CO_2 ratio at 300 °C, 2.0 MPa.

	Impregnating pH	**Activity**	**Selectivity**	**Activity**	**Selectivity**
		GHSV: 1 mL g^{-1} s^{-1}		**GHSV: 5 mL g^{-1} s^{-1}**	
Standard Synthesis	5.9	20.6%	90.6%	14.1%	97.2%
Acidified Synthesis	4.0	19.2 %	88%	13.6%	97.2%

4.6 Shelf Life

In addition to the influence of synthetic conditions, the stability of a catalyst under ambient storage is also important in the practical application of the material. The best performing catalyst in this work, non-calcined with a molar ratio of 1/4/15 (K/Mo/Al_2O_3), provided a CO yield of 18.7% when tested within two

weeks of synthesis (See Table 2). However, after being stored at ambient conditions for 15 months, the same catalyst produced a CO yield of 8.9% under identical conditions.

In an attempt to regenerate the catalyst, the 15-month-old K-Mo_2C@γ-Al_2O_3 was re-carburized under conditions identical to the original catalyst synthesis. Figure 7 displays the X-ray diffraction patterns for the fresh, aged, and re-carburized catalyst. The aged sample clearly displays a loss of crystalline Mo_2C, likely due to gradual oxidation of the active Mo_2C surface with time.[46] Upon re-carburization, the sample displayed reflections corresponding to Mo_2C which were of greater intensity relative to the "aged" sample. However, the relative intensity of these reflections remained less than the original "Fresh" catalyst, indicating complete re-carburization was not achieved. When tested under identical conditions, the "re-carburized" catalyst provided an improved CO yield of 15.9%, demonstrating a straightforward route to catalyst regeneration.

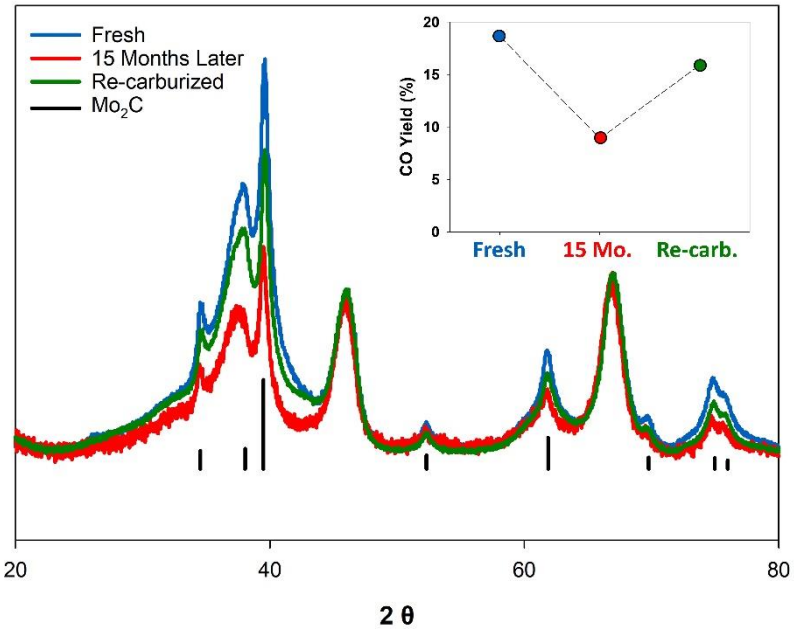

Figure 7. X-ray diffraction patterns normalized to the γ-Al_2O_3 signal for "Fresh" (blue), "Aged" (red), and "Re-carburized" (green) K-Mo_2C@γ-Al_2O_3. Inset: CO Yield observed for the three catalysts under identical conditions.

5.0 Conclusions

Potassium promoted molybdenum carbide is an effective catalyst for the low temperature reverse water gas shift (RWGS) reaction, which can be considered an important step in the overall reduction of CO_2 to liquid fuels and other chemicals. To optimize the performance of K-Mo_2C@γ-Al_2O_3 for the RWGS reaction, systematic evaluation of various parameters such as support dependence, catalyst loading, calcination temperature, carburization conditions, impregnating pH, and catalyst stability under ambient conditions were performed.

Besides providing a high surface area for the dispersion of Mo_2C, it was demonstrated that the γ-Al_2O_3 support has an important influence on the carburization of the K-Mo precursor, enabling a direct route to

temperature programmed carburization to Mo_2C, which could not be achieved with the K-Mo precursor alone. Calcination of the supported K-Mo precursor prior to carburization was found to be slightly detrimental to catalyst performance, with the non-calcined catalyst displaying the greatest degree of carburization and RWGS activity. Optimal loading of the K and Mo precursors on the γ-Al_2O_3 support was found to consist of molar ratios of 1/4/15 (K/Mo/Al_2O_3) respectively, which corresponded to the smallest observable reflections for Mo_2C as observed by X-ray diffraction. Extensive carburization of the molybdenum precursors was found to have no effect on catalyst performance, indicating no significant buildup of polymeric carbon. Decreasing the pH of the impregnating solution was found to have no effect on the catalyst's overall performance. Finally, K-Mo_2C@γ-Al_2O_3 was found to display a "shelf life", with catalyst performance degrading after being stored under ambient conditions for 15 months. Upon re-carburization, the catalyst performance was improved, providing CO yields close to the freshly synthesized material.

6.0 Recommendations

Using the results outlined in this manuscript, we offer the following insights and recommendations in regards to the optimized synthesis of K-Mo_2C as a catalyst for the reverse water gas shift reaction:

1. γ-Al_2O_3 serves as an effective support by providing a large surface area for the active Mo_2C catalyst, and by enabling a straightforward synthetic route to K-Mo_2C. Studies aimed at further understanding the catalytically relevant interaction between K-Mo_2C and Al_2O_3, as well as other supports, are recommended.

2. Calcination of the potassium and molybdenum precursors prior to the K-Mo_2C synthesis was found to be detrimental to the material's activity for the reverse water gas shift reaction. Accordingly, we recommend calcination should be avoided in the synthesis of this catalytic material.

3. The Mo precursor used in this study (ammonium molybdate) likely generates ammonia gas under the carburization conditions used in this work. Accordingly, we recommend avoiding the use of quartz tubes for the carburization of this precursor, as this vapor can degrade quartz under elevated temperatures.

4. We recommend the following standardized protocol for the synthesis of K-Mo_2C@Al_2O_3 at the laboratory scale: Carburization of 4 g of precursor in 20% CH_4 in H_2 at 600 °C, at a total gas flow rate of 0.3 L min^{-1} for a total of 4 hours (corresponding to a total gas flow of 18 L g^{-1}), followed by passivation in a 1% O_2 /99% N_2 blend at room temperature overnight. No hydrogen treatment step is required under these conditions.

5. The catalyst composed of molar ratios of 1/4/15, K/Mo/Al_2O_3 was found to be the most active for the RWGS reaction. Accordingly, these ratios are recommended for future use.

6. Catalyst activity was found to decline after storage under ambient conditions. It is recommended that catalysts be stored under inert environments, or used within two weeks of synthesis. Alternatively, the catalyst can be re carburized following extended ambient oxidation.

7.0 Acknowledgements

This work was supported by the Office of Naval Research.

8.0 References

1. Department of Defense. Operational Energy Strategy. 2016. Available online: http://www.acq.osd.mil/eie/Downloads/OE/2016%20DoD%20Operational%20Energy%20Strategy%20WEBc.pdf (accessed on 28 January 2022). (2016).

2. National, G. & Pillars, H. Summary of the 2018 National Defesne Strategy of the United States of America. Available online: https: //dod.defense.gov/Portals/1/Documents/pubs/2018-National-Defense-Strategy-Summary.pdf (accessed on 28 January 2022)

3. National Defense Authorization Act for Fiscal Year 2020, H.R. 2500, 116th Cong. (2019-2020). Available online: https://www.congress.gov/bill/116th-congress/house-bill/2500 (accessed on 28 January 2022).

4. Dorner, R., Hardy, D. & Williams, F. Influence of Gas Feed Composition and Pressure on the Catalytic Conversion of CO2 to Hydrocarbons Using a Traditional Cobalt-Based Fischer- Tropsch Catalyst. *Energy & Fuels* **23,** 4190–4195 (2009).

5. Willauer, H. D., Hardy, D. R., Lewis, M. K., Ndubizu, E. C. & Williams, F. W. Effects of pressure on the recovery of CO2 by phase transition from a seawater system by means of multilayer gas permeable membranes. *J. Phys. Chem. A* **114,** 4003–4008 (2010).

6. Willauer, H. D., Dimascio, F., Hardy, D. R. & Williams, F. W. Feasibility of CO2 extraction from seawater and simultaneous hydrogen gas generation using a novel and robust electrolytic cation exchange module based on continuous electrodeionization technology. *Ind. Eng. Chem. Res.* **53,** 12192–12200 (2014).

7. Willauer, H. D., DiMascio, F., Hardy, D. R., Lewis, M. K. & Williams, F. W. Development of an Electrochemical Acidification Cell for the Recovery of CO_2 and H_2 from Seawater. *Ind. Eng. Chem. Res.* **50,** 9876–9882 (2011).

8. Willauer, H. D., Dimascio, F., Hardy, D. R., Lewis, M. K. & Williams, F. W. Development of an electrochemical acidification cell for the recovery of CO2 and H2 from seawater II. Evaluation of the cell by natural seawater. *Ind. Eng. Chem. Res.* **51,** 11254–11260 (2012).

9. Willauer, H. D., DiMascio, F., Hardy, D. R. & Williams, F. W. Development of an Electrolytic Cation Exchange Module for the Simultaneous Extraction of Carbon Dioxide and Hydrogen Gas from Natural Seawater. *Energy & Fuels* **31**, 1723-1730 (2017).

10. Willauer, H. D., Hardy, D. R., Lewis, M. K., Ndubizu, E. C. & Williams, F. W. Extraction of CO2 from

seawater and aqueous bicarbonate systems by ion-exchange resin processes. *Energy and Fuels* **24,** 6682–6688 (2010).

11. Porosoff, M. D., Yan, B. & Chen, J. G. Catalytic reduction of CO2 by H2 for synthesis of CO, methanol and hydrocarbons: challenges and opportunities. *Energy Environ. Sci.* **9,** 62 (2016).

12. Daza, Y. & Kuhn, J. N. CO2 conversion by reverse water gas shift catalysis: Comparison of catalysts and mechanisms and their consequences for CO2 conversion to liquid fuels. *RSC Adv.* **6,** 49675–49691 (2016).

13. Ma, Z. & Porosoff, M. D. Development of Tandem Catalysts for CO 2 Hydrogenation to Olefins. *ACS Catal.* **9,** 2639–2656 (2019).

14. Wang, W., Wang, S., Ma, X. & Gong, J. Recent advances in catalytic hydrogenation of carbon dioxide. *Chem. Soc. Rev.* **40,** 3703 (2011).

15. Chen, C. S., Cheng, W. H. & Lin, S. S. Study of iron-promoted Cu/SiO2catalyst on high temperature reverse water gas shift reaction. *Appl. Catal. A Gen.* **257,** 97–106 (2004).

16. Chen, C. S., Cheng, W. H. & Lin, S. S. Enhanced activity and stability of a Cu/SiO2 catalyst for the reverse water gas shift reaction by an iron promoter. *Chem. Commun.* **1,** 1770–1771 (2001).

17. Su, X., Yang, X., Zhao, B. & Huang, Y. Designing of highly selective and high-temperature endurable RWGS heterogeneous catalysts: recent advances and the future directions. *J. Energy Chem.* **26,** 854–867 (2017).

18. Willauer, H. D. *et al.* Evaluation of CO2 Hydrogenation in a Modular Fixed-Bed Reactor Prototype. *Catalysts* **10,** 970 (2020).

19. Juneau, M. *et al.* Assessing the viability of K-Mo2C for reverse water-gas shift scale-up: Molecular to laboratory to pilot scale. *Energy Environ. Sci.* **13,** 2524–2539 (2020).

20. Patterson, P. M., Das, T. K. & Davis, B. H. Carbon monoxide hydrogenation over molybdenum and tungsten carbides. *Appl. Catal. A Gen.* **251,** 449–455 (2003).

21. Oshikawa, K., Nagai, M. & Omi, S. Characterization of molybdenum carbides for methane reforming by TPR, XRD, and XPS. *J. Phys. Chem. B* **105,** 9124–9131 (2001).

22. Claridge, J. B. *et al.* New Catalysts for the Conversion of Methane to Synthesis Gas : Molybdenum and Tungsten Carbide. *J. Catal.* **100,** 85–100 (1998).

23. Porosoff, M. D., Yang, X., Boscoboinik, J. A. & Chen, J. G. Molybdenum Carbide as Alternative Catalysts to Precious Metals for Highly Selective Reduction of CO2 to CO. *Angew. Chemie* **126,** 6823–6827 (2014).

24. Gnanamani, M. K., Hamdeh, H. H., Shafer, W. D., Hopps, S. D. & Davis, B. H. Hydrogenation of carbon dioxide over iron carbide prepared from alkali metal promoted iron oxalate. *Appl. Catal. A Gen.* **564,** 243–249 (2018).

25. Woo, H. C., Park, K. Y., Kim, Y. G., Namau]Jong ShikChung, I. S. & Lee, J. S. Mixed alcohol synthesis from carbon monoxide and dihydrogen over potassium-promoted molybdenum carbide catalysts. *Appl. Catal.* **75,** 267–280 (1991).

26. Morse, J. R., Juneau, M., Baldwin, J. W., Porosoff, M. D. & Willauer, H. D. Alkali promoted

tungsten carbide as a selective catalyst for the reverse water gas shift reaction. *J. CO2 Util.* **35,** 38–46 (2020).

27. Porosoff, M. D., Baldwin, J. W., Peng, X., Mpourmpakis, G. & Willauer, H. D. Potassium-Promoted Molybdenum Carbide as a Highly Active and Selective Catalyst for CO2 Conversion to CO. *ChemSusChem* **10,** 2408–2415 (2017).

28. Porosoff, M. & Willauer, H. D. Alkali metal doped molybdenum carbide supported on gamma-alumina for selective CO2 hydrogenation into CO. US 2019/0329227 A1, (2019).

29. Ro, I., Resasco, J. & Christopher, P. Approaches for Understanding and Controlling Interfacial Effects in Oxide-Supported Metal Catalysts. *ACS Catal.* **8,** 7368–7387 (2018).

30. Munnik, P., De Jongh, P. E. & De Jong, K. P. Recent Developments in the Synthesis of Supported Catalysts. *Chem. Rev.* **115,** 6687–6718 (2015).

31. Christensen, J. M. *et al.* Catalytic conversion of syngas into higher alcohols over carbide catalysts. *Ind. Eng. Chem. Res.* **51,** 4161–4172 (2012).

32. Kojima, R. & Aika, K. I. Molybdenum nitride and carbide catalysts for ammonia synthesis. *Appl. Catal. A Gen.* **219,** 141–147 (2001).

33. Said, A. A. Mutual influences between ammonium heptamolybdate and γ-alumina during their thermal treatments. *Thermochim. Acta* **236,** 93–104 (1994).

34. Vo, D. V. N. & Adesina, A. A. Kinetics of the carbothermal synthesis of Mo carbide catalyst supported on various semiconductor oxides. *Fuel Process. Technol.* **92,** 1249–1260 (2011).

35. Shimada, H., Sato, T., Yoshimura, Y., Hiraishi, J. & Nishijima, A. Support effect on the catalytic activity and properties of sulfided molybdenum catalysts. *J. Catal.* **110,** 275–284 (1988).

36. Thomazeau, C., Martin, V. & Afanasiev, P. Effect of support on the thermal decomposition of (NH4)6Mo7O24·4H2O in the inert gas atmosphere. *Appl. Catal. A Gen.* **199,** 61–72 (2000).

37. Lee, J. S., Oyama, S. T. & Boudart, M. Molybdenum Carbide Catalysts. *J. Catal.* **106,** 125–133 (1987).

38. Ribeiro, F. H., Betta, R. A. D., Guskey, G. J. & Boudart, M. Preparation and Surface Composition of Tungsten Carbide Powders with High Specific Surface Area. *Chem. Mater.* 805–812 (1991). doi:10.1021/cm00017a015

39. Li, S., Kim, W. B. & Lee, J. S. Effect of the Reactive Gas on the Solid-State Transformation of Molybdenum Trioxide to Carbides and Nitrides. *Chem. Mater.* **10,** 1853–1862 (1998).

40. Lee, J. S., Oyama, S. T. & Boudart, M. Molybdenum Carbide Catalysts 1. Synthesis of Unsupported Powders. *J. Catal.* **106,** 125–133 (1987).

41. Moreau, F., Bond, G. C. & Taylor, A. O. Gold on titania catalysts for the oxidation of carbon monoxide: Control of pH during preparation with various gold contents. *J. Catal.* **231,** 105–114 (2005).

42. Fountzoula, C., Spanos, N., Matralis, H. K. & Kordulis, C. Molybdenum-titanium oxide catalysts: The influence of the preparation conditions on their activity for the selective catalytic reduction of NO by NH3. *Appl. Catal. B Environ.* **35,** 295–304 (2002).

43. Bergwerff, J. A. *et al.* Envisaging the physicochemical processes during the preparation of supported catalysts: Raman microscopy on the impregnation of Mo onto Al2O3 extrudates. *J. Am. Chem. Soc.* **126,** 14548–14556 (2004).

44. Jiao, L. & Regalbuto, J. R. The synthesis of highly dispersed noble and base metals on silica via strong electrostatic adsorption: I. Amorphous silica. *J. Catal.* **260,** 329–341 (2008).

45. Kosmulski, M. The pH-dependent surface charging and points of zero charge. V. Update. *J. Colloid Interface Sci.* **353,** 1–15 (2011).

46. Mehdad, A., Jentoft, R. E. & Jentoft, F. C. Passivation agents and conditions for Mo2C and W2C: Effect on catalytic activity for toluene hydrogenation. *J. Catal.* **347,** 89–101 (2017).